Dissipative Topological Dynamics in Optical Waveguides: Sensitivity versus Robustness

Zhiyuan Lin,[1] Jian Li,[1] Wange Song,[1,*] Shanhe Su,[2] Jiacheng Sun,[1] Shengjie Wu,[1] Chunyu Huang,[1] Shining Zhu,[1] and Tao Li[1,†]

[1]National Laboratory of Solid State Microstructures, Key Laboratory of Intelligent Optical Sensing and Manipulations, Jiangsu Key Laboratory of Artificial Functional Materials, School of Physics, College of Engineering and Applied Sciences, Nanjing University, Nanjing, 210093, China

[2]Department of Physics, Xiamen University, Xiamen, 361005, China

(Received 9 January 2025; revised 23 March 2025; accepted 12 May 2025; published 4 June 2025)

Topological physics has garnered attention across various fields, emphasizing topologically protected modes renowned for their robustness against disorders. Recent advancements have expanded from conservative wave systems to diffusion systems with dissipative interactions. However, the transition region between wave and diffusion dynamics remains scarce, primarily due to the complexities involved in coupling modulation. Here, we develop a universal coupling control scheme via reservoir engineering, achieving conservative, dissipative, and mixed topologies in an optical waveguide array. Contrary to the belief that topological modes are disorder resistant, we found that topological dissipative modes are highly sensitive to initial excitations and noise. This sensitivity is due to their residence within the complex band gap, facilitating the excitation and preservation of bulk modes with lower loss. We also propose a method to control the degree of topological robustness and even stabilize these sensitive topological states by selectively managing dissipative potentials. Our Letter offers new insights into the dissipative dynamics of topological states, paving the way for wave coherent manipulation and diffusion transport on photonic chips.

DOI: 10.1103/bk7q-6r9d

Topological phases of matter, initially discovered in solid-state physics, have been extended to classical wave systems such as acoustics and photonics due to the similarity between the field equation and the Schrödinger equation [1–12]. One of the fundamental topological concepts is the bulk-boundary correspondence [13–15], which is crucial in topological theory. This principle relates to bulk topological invariants [14,16] and predicts the presence of topologically protected edge states at the boundaries. The topological edge states are notable for their robustness against disorder, attracting significant attention for robust wave manipulations, such as Floquet topological insulators [17–22], topological pumping [23–27], higher-order topology [28–32], non-Hermitian topology [33–41], non-Abelian effects [42–47], and topological lasers [48–50], etc. This robustness is traditionally considered an inherent property determined by the topological invariant, which can only be altered through a topological phase transition associated with closing a gap. Nonetheless, it is also realized that the nontrivial topological invariant does not imply robustness of all relevant features of the topological states [51,52].

Most systems demonstrating topological phenomena rely on conservative couplings, intrinsically determined by direct mode overlap [53]. However, dissipative couplings also exist in physics, particularly described by the dissipation term of the master equation in open quantum systems, yielding unique dissipative topological properties [37,54–64]. Recently, diffusion systems, such as heat transport, have garnered attention for their intriguing diffusion effects like thermal cloaking [65,66], illusions [67], and coding [68]. Couplings in diffusion systems are

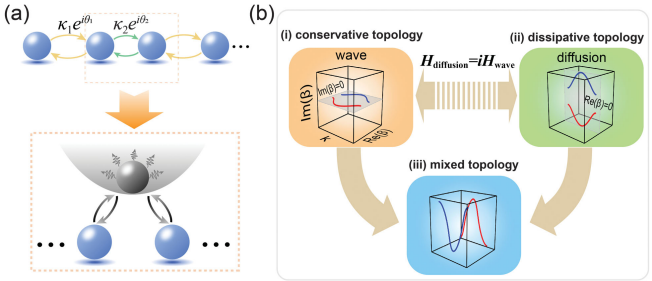

FIG. 1. (a) The schematic of SSH model with complex couplings $\kappa_n \exp(i\theta_n)$ $(n = 1, 2)$ and the scheme for obtaining complex coupling via the intermediate reservoir engineering. (b) Classification of the topology according to complex couplings and their unique dynamics, including (i) conservative (CT), (ii) dissipative (DT), and (iii) mixed topology (MT), which are classified by the coupling phases $\theta_{1,2}$, and the trivial or nontrivial topology is determined by the coupling amplitude difference $\delta\kappa$.

*Contact author: songwange@nju.edu.cn
†Contact author: taoli@nju.edu.cn

inherently dissipative, with the corresponding Hamiltonian being anti-Hermitian with imaginary eigenspectra (Fig. 1), which indicates that fields in diffusion systems are governed by "decay," showcasing completely distinct dynamics and topological physics [6,7,15,69–71]. Although topology in wave and diffusion systems has been systematically studied separately, a general framework bridging their topological dynamics between conservative and dissipative remains elusive. Observing such mixed topology edge states is still challenging due to the essential control of the non-Hermitian complex couplings.

Here, we propose a scheme to endow the topological system with wave and diffusion properties via coupling control by introducing common reservoir engineering [56,57,63] in an optical waveguide array. We observe unique dynamics of topological modes when transitioning from conservative to dissipative topology. The robustness of the edge state is maintained only in the conservative topology regime and becomes anomalously sensitive in the dissipative topological states. This is because topological dissipative modes are always in the complex (Re/ Im) band gap, leading to easier excitation of bulk modes with lower loss. Moreover, we propose an effective approach to control the topological robustness freely and even stabilize these sensitive topological states by dissipation engineering in the lattice. This Letter uncovers the subtle relationship between conservative and dissipation topology, opening new avenues for light coherent manipulation and diffusion transport.

We start with the celebrated Su-Schrieffer-Heeger (SSH) model with complex couplings $C_n = \kappa_n \exp(i\theta_n)$ ($n = 1$, 2) to illustrate the concept [see Fig. 1(a)]. Different from the traditional SSH model, the couplings between neighboring sites here are complex and non-Hermitian, i.e., $C_{ji} \neq C_{ij}^*$ ($\theta_{1,2} \neq 0$). Such coupling arrangements can be obtained indirectly by coupling to a common reservoir (Supplemental Material S1 and S2 [72]), in which some information or energy is lost to the reservoir during the coupling process. The full dynamics of such a system can be described by the general Lindblad master equation $\mathrm{d}\rho/\mathrm{d}t = \Lambda\rho$ (Supplemental Material S3 [72]), where the Liouvillian ($\Lambda = \mathrm{K} + \Delta$) contains the coherent (K) and dissipative (Δ) parts [75,76]. The system exhibits only coherent ($\mathrm{d}\rho/\mathrm{d}t = \mathrm{K}\rho$) or diffusion ($\mathrm{d}\rho/\mathrm{d}t = \Delta\rho$) dynamics when the couplings become purely real (e.g., $\theta_{1,2} = 0$) or imaginary (e.g., $\theta_{1,2} = \pi/2$), respectively. When $\theta_{1,2}$ takes other values, one obtains complex couplings whose dynamics are governed by the full master equation, serving as a bridge between the conservative and dissipative dynamics. These coupling arrangements motivate three different topological classifications [see Fig. 1(b)], i.e., conservative (CT), dissipative (DT), and mixed topology (MT), tailored to their unique dynamics and energy band structures.

For such a non-Hermitian SSH model, its bulk Hamiltonian is

$$H(k) = \left[\kappa_1 e^{i\theta_1} + \kappa_2 e^{i\theta_2}\cos(ka)\right]\sigma_x - \kappa_2 e^{i\theta_2}\sin(ka)\sigma_y, \quad (1)$$

which possesses a chiral symmetry $[\sigma_z H(k)\sigma_z = -H(k)]$ and the energy spectrum is symmetric around the zero energy [77], here σ_i ($i = x$, y, z) are Pauli matrices. The topology of this system can be characterized by the winding number $\mathcal{W}$, which is determined by the amplitude of the couplings $\kappa_{1,2}$ ($\mathcal{W} > 1$ when $\delta\kappa < 0$ and $\mathcal{W} = 0$ when $\delta\kappa > 0$, where $\delta\kappa = \kappa_1 - \kappa_2$, where $\kappa_{1,2}$ are real positive numbers). Notably, the winding number defined in the parameter space in the Hermitian case is relative to the coordinate origin $O(0, 0)$, which, however, splits into two exceptional points (EPs) determined by the coupling amplitude and phase [$\mathrm{EP}_{1,2}$: $(0, \pm\kappa_1 \sin(\delta\theta))$, $\delta\theta = \theta_1 - \theta_2$] in this specific non-Hermitian arrangement (Supplemental Material S4 [72]). Encircling an exceptional point yields a winding number of $1/2$. This induces new topological phase transitions compared to the Hermitian counterpart and the trivial or nontrivial topology is determined by the coupling amplitude difference $\delta\kappa$.

To get into the unique properties of the general mixed topology, we construct a domain wall between topologically trivial ($\delta\kappa = \kappa_2 - \kappa_1 > 0$) and nontrivial ($\delta\kappa = \kappa_1 - \kappa_2 < 0$) non-Hermitian chains, as shown in Fig. 2(a). By properly tuning the coupling phases $\theta_{1,2}$ ($0 \leqslant \theta_{1,2} < 2\pi$), we can achieve continuous transition from conservative to mixed, and to dissipative topology. For example, $\theta_{1,2} = 0(\pi)$ and $\theta_{1,2} = \pi/2$ ($3\pi/2$) correspond to conservative and dissipative topology, respectively, while the remaining case corresponds to general mixed topology. Without losing generality, here θ_2 is fixed to 0 and we alter the coupling phase $\theta_1 = \theta$. The energy spectrum in the Re/ Im planes is illustrated in Fig. 2(b), where the imaginary part $\mathrm{Im}(\varepsilon) > 0$ indicates gain and $\mathrm{Im}(\varepsilon) < 0$ indicates loss. This model can be implemented in a passive scheme by applying a global loss without introducing additional gain, while still maintaining the topological properties [39]. The topological zero modes are always in the band gap formed by the periodically twisted bulk bands as the coupling phase θ changes. These zero modes have the same degree of localizations, characterized by equal inverse participation ratios (IPRs), but possess different phase distributions endowed by the non-Hermitian couplings (Supplemental Material S5 [72]).

We next consider the dynamic properties of the zero modes. In general, the dynamics is governed by $|\varphi(z)\rangle = \mathrm{T}\exp(-i\int_0^z H(z')dz')|\varphi(0)\rangle$, where T is the time-ordering operator. When the excitation field is the exact zero mode, i.e., $|\varphi(0)\rangle = |\varphi_{\mathrm{ZM}}\rangle$ the occupation remains constant during evolution for all θ since the Hamiltonian is z independent, i.e.,$|\varphi(z)\rangle = \exp(-i\varepsilon z)|\varphi_{\mathrm{ZM}}\rangle = |\varphi_{\mathrm{ZM}}\rangle$. However, things become interesting if the initial state slightly deviates from the perfect zero mode, which is unavoidable in real-world

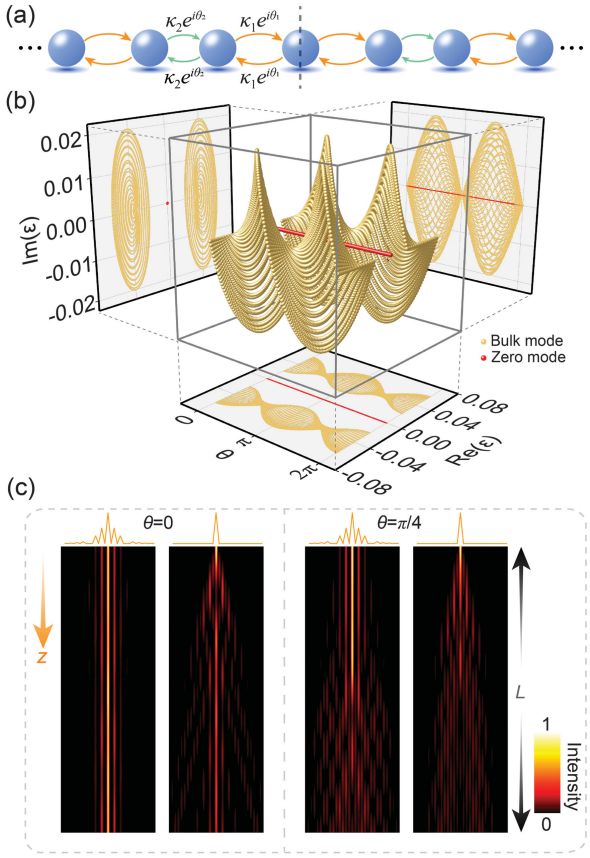

FIG. 2. (a) A domain wall formed by the topologically trivial or nontrivial SSH chains. The interface coupling is set as $\kappa_{in} = \kappa_1 \exp(i\theta_1)$. (b) Energy spectrum with projections in the complex plane as a function of the coupling phase $\theta_1 = \theta$. (c) Evolution dynamics of the zero modes with different excitations (exact zero mode with perturbation and single-site excitations) and coupling phases ($\theta = 0$, $\pi/4$), here $\theta_2 = 0$, $\kappa_2 = 2\kappa_1$, and $L = 5L_0$, where $L_0 = \pi/\kappa_2$. The intensity is normalized to 1 at every z for clearer presentation.

experiments. First, we consider the excitation commonly used in practice, i.e., the single-site excitation. As shown in Fig. 2(c), most energy is localized at the interface for the traditional or Hermitian case $\theta = 0$, whereas an unexpected deviation from the zero mode occurs and the energy quickly diffuses throughout the system for mixed case $\theta = \pi/4$. To further evaluate the influence of the deviation from the exact eigenmodes, we impose a slight perturbation $|\delta\varphi\rangle$ to the perfect zero-mode initial state, i.e.,$|\varphi(0)\rangle = |\varphi_{ZM}\rangle + |\delta\varphi\rangle$, as the input states. Note that this initial state is very close to the zero mode $|\langle\varphi_{ZM}|\varphi(0)\rangle|^2 \approx 0.98$ (0.6 for single-site excitation and 1 for perfect excitation). The evolution holds the zero-modes' localization property for the traditional or Hermitian case $\theta = 0$ ($|\varphi(z)\rangle \approx |\varphi_{ZM}\rangle$), while it deviates completely from the zero mode for mixed case $\theta = \pi/4$ after propagating a distance, even though the perturbation is very slight [Fig. 2(c)]. This implies that for the mixed topology, although there are zero modes in the gap (still inherent topological protection), this protection will not guarantee their robustness in dynamic evolutions. Since the topological mode of the system always resides within the gap of the complex energy plane, any deviation of the initial state from the perfect topological mode can easily excite bulk modes with lower losses [larger $\mathrm{Im}(\varepsilon)$], which is the primary source of sensitivities in the system (see Supplemental Material S6 [72]).

To experimentally verify the aforementioned phenomenon of mixed topology, it is essential to accurately implement the complex couplings. However, achieving complex couplings is not straightforward, let alone exerting precise control over them. Here we employ an optical waveguide system based on a thin film lithium niobate (TFLN) platform. The required universal complex coupling control can be achieved by adding an auxiliary waveguide ("C") with complex detuning to the intermediate of the two main waveguides ("A" and "B"), where the effective coupling ($\kappa e^{i\theta}$) between the main waveguides can be obtained by changing the complex detuning, i.e., the width of waveguide (w_a) and chromium (Cr, w_{Cr}) [Fig. 3(a)] when adiabatically eliminating auxiliary site. We experimentally demonstrate this universal coupling control, including negative, dissipative, and general complex couplings, supported by solid experimental data that verifies the achievement of arbitrary coupling strength and coupling phase across half of the complex coupling plane (see Supplemental Material S2 for detailed experimental data [72]). Our experimental optical lattice comprised 31 lithium niobate waveguides on the SiO_2 substrate with air cladding, as shown in Fig. 3. The main waveguide width is $w = 800$ nm and the height is $h = 300$ nm. The loss is introduced by coating a layer of Cr on auxiliary waveguides with fixed thickness $h_{Cr} = 20$ nm but different width w_{Cr} for desired loss. Waveguide spacing between the main and auxiliary (main) waveguides is $g_1 = 580$ nm ($g_2 = 710$ nm). The scanning electron microscope (SEM) pictures of experimentally fabricated samples are shown in Fig. 3(b), where the deposited Cr can be clearly observed from the enlarged picture at the bottom panel.

Three types of samples ($\theta = 0$, $\pi/4$, and $\pi/2$) were fabricated, each with distinct different propagation lengths ($L = 50$, 100, 150, 200, 250, and 300 μm) to capture various stages of mode evolutions. For each waveguide lattice, a near-infrared laser (wavelength $\lambda = 1550$ nm) is incident into a grating coupler to excite the central site of the waveguide array, and the output signal is scattered from the end of the waveguides into free space, collected by a near-infrared charge-coupled device camera [right panel in Fig. 3(a)]. The theoretical and experimental results for these three arrangements are demonstrated in Fig. 3(c). When there are only conservative couplings, i.e., $\theta = 0$, it features the traditional conservative topology and the light mainly localized at the interface regardless of the evolutionary distance, as shown in Fig. 3(c)(i). When the coupling enters

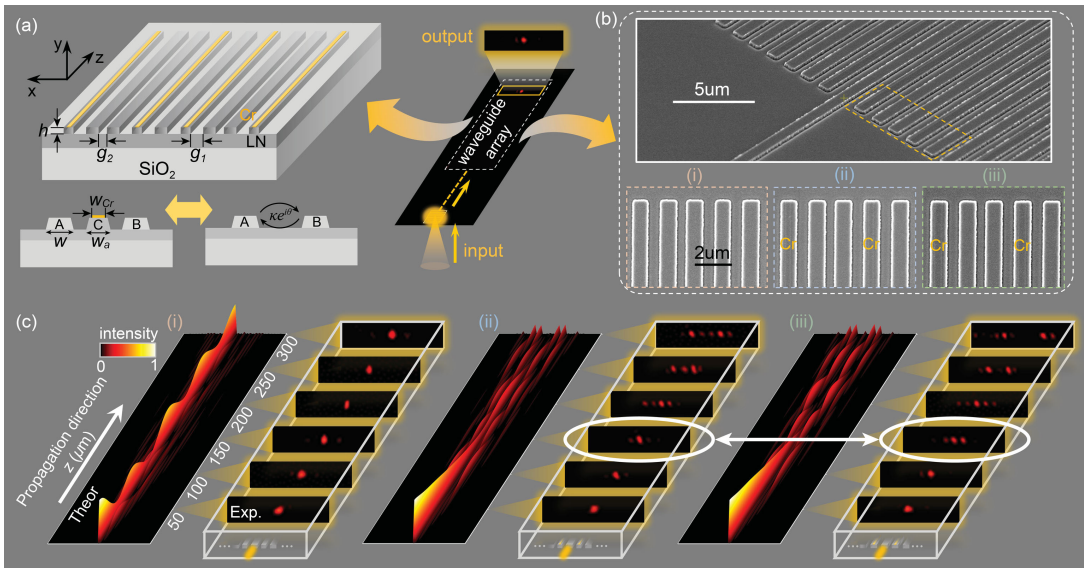

FIG. 3. Realization of mixed topological states in on-chip lithium niobate photonics. (a) Schematic of the lithium niobate waveguide design (left panel). The complex coupling between main waveguides (marked by "A" and "B") is introduced by an auxiliary waveguide (marked by "C") with complex detuning engineering by changing the width of waveguide (w_a) and Cr (w_{Cr}). In the experiment, the input light is coupled from the grating to the array and scattered from the end of the waveguides into free space, collected by a near-infrared charge-coupled device camera (right panel). (b) SEM image of one of the experimentally fabricated samples. The bottom panels show enlarged views of three cases, corresponding to (i) $\theta = 0$, (ii) $\theta = \pi/4$, and (ii) $\theta = \pi/2$. Cr strips can be clearly observed. (c) The theoretical results (left) and experimentally measured light intensities (right) at different lengths for three arrangements in (b), where the white ellipses have been added in (ii) and (iii) to emphasize the evolution differences. Other parameters are $w = 800$, $h = 300$, $h_{Cr} = 20$, $g_1 = 580$, $g_2 = 710$ nm.

the complex region (e.g., $\theta = \pi/4$) or becomes purely dissipative ($\theta = \pi/2$), the evolution becomes intricate, as shown in Figs. 3(c)(ii) and 3(c)(iii). For short lengths (e.g., $L = 50$ and 100 μm), light remains primarily localized at the interface in both cases. However, when the length is increased to $L = 150$ μm, subtle differences emerge: light decays slowly and remains at the interface (the center waveguide) for complex coupling, while a significant amount of light diffuses into the adjacent bulk waveguides for the purely dissipative case [indicated by the white ellipses in Figs. 3(c)(ii) and 3(c)(iii)], which is consistent with the simulations. This result is related to the difference in band structures (Fig. 2), where the critical length for maintaining topological modes at the interface is determined by the imaginary parts of the spectra (see details in Supplemental Material S6 [72]). When the distance becomes sufficiently long (e.g., $L > 200$ μm), light no longer remains coherently localized at the interface in either case, but gradually diffuses from the interface into the bulk waveguides.

We next show how to restore the dynamic stability of the sensitive topological mode and endow them with different levels of robustness by tuning the dissipation level of topological modes with respect to the bulk modes. In this spirit, we selectively apply another set of dissipation distribution Γ to the main site "A" for the complex-coupling case, e.g., $\theta = \pi/4$ [Fig. 4(a)], the bulk Hamiltonian becomes

$$H'(k) = \left[\kappa_1 e^{i\theta_1} + \kappa_2 e^{i\theta_2}\cos(ka)\right]\sigma_x - \kappa_2 e^{i\theta_2}\sin(ka)\sigma_y - i\Gamma\frac{\sigma_z + \sigma_0}{2}, \quad (2)$$

where σ_0 is a unitary matrix. Although the introduction of the dissipation (Γ) in Eq. (2) breaks chiral symmetry, the zero modes can still exist because the dissipation is applied to sites where the zero modes are not distributed, thus only breaking the symmetry of the bulk modes. As dissipation increases, the bulk modes become more lossy (shifting further in the negative direction of the imaginary part, as indicated by the dashed arrows), while the zero mode remains unchanged. During this process, the dynamics of the zero modes gradually become more localized (see Supplemental Material S7 and Video 1 [72]), indicating that the topological robustness is enhanced. Results of controlling different levels of robustness (quantified by the zero-mode fidelity $f = |\langle\varphi_{ZM}|\varphi(z)\rangle|$) by onsite dissipation Γ are illustrated in Fig. 4(b). For $\Gamma = 0$, there is a significant decay of fidelity when the evolution distance exceeds a critical length. As the dissipation increases, the critical length of the fidelity increases, implying gradually enhanced robustness. When the dissipation is large enough ($> 0.5\kappa_2$), the fidelity approaches 1 and remains stable.

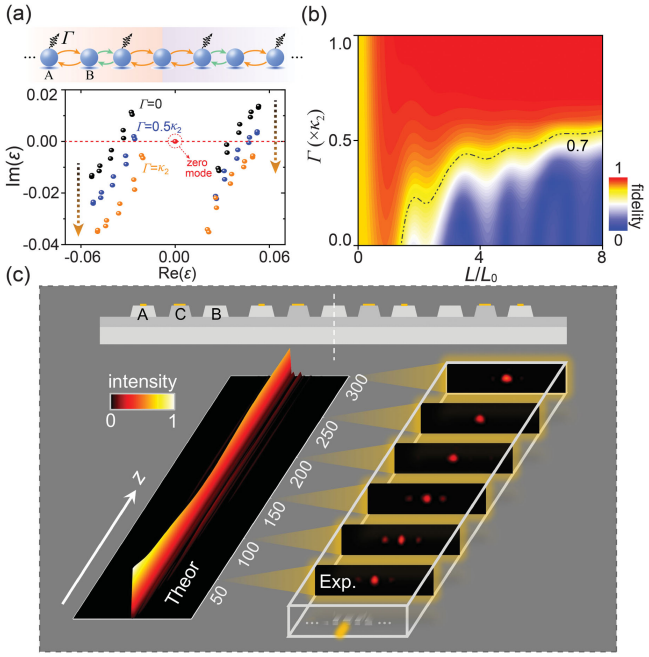

FIG. 4. Retrieve the dynamic stability of the topological dissipative mode. (a) Schematic of the SSH model with complex couplings ($\theta = \pi/4$) and alternate onsite dissipation Γ (top panel), and the eigenenergy with different onsite dissipation ($\Gamma = 0$, $0.5\kappa_2$, and κ_2) in the complex plane. (b) Fidelity of zero mode as a function of evolution distance L and onsite dissipation Γ with single-site excitation. (c) Schematic of the lithium niobate waveguide design, where additional Cr (200 nm wide) is deposited on top of main waveguides ("A") to introduce desired onsite dissipation (top panel). Bottom panel: the theoretical results ($\Gamma = \kappa_2$) and experimentally measured light intensities. Other parameters are the same as that of $\theta = \pi/4$ in Fig. 3.

Experimental verification of the robustness enhancement is shown in Fig. 4(c), where parameters are the same as that of $\theta = \pi/4$ in Fig. 3, except for the additional onsite dissipation introduced by depositing Cr (200 nm wide) on top of the main waveguides ("A"), which corresponds to the case $\Gamma = \kappa_2$ in Fig. 4(b). In contrast to the results in Fig. 3(c)(ii), where much energy diffuses from the interface into the bulk waveguides, light in Fig. 4(c) mainly localized at the domain wall and becomes more stable as the distance increases.

In conclusion, we have delved into the mixed (wave and diffusive) topology based on an optical waveguide array. We experimentally validated perturbation-sensitive topological dissipative modes through a universal coupling control scheme. This sensitivity arises from the band structure of the topological system, wherein the topological modes consistently reside within the complex band gap. Consequently, bulk modes with lower loss can be easily excited if the state strays from the ideal topological mode. This finding also suggests a method to control the robustness of topological states and we can restore the dynamic stability of the topological dissipative mode by selectively applying onsite dissipation. Our Letter enhances the understanding of non-Hermitian topology and offers new insights into leveraging the robustness of topological modes through dissipation, the coupling control scheme in lithium niobate photonics opens up new possibilities for innovative on-chip light manipulation.

Acknowledgments—The authors acknowledge the financial support from The National Key R&D Program of China (No. 2023YFA1407700), National Natural Science Foundation of China (No. 62288101, No. 62325504, No. 12204233, No. 12174186, and No. 92250304). T. L. thanks the support from Dengfeng Project B of Nanjing University.

Data availability—No data were created or analyzed in this study.

[1] A. B. Khanikaev, S. H. Mousavi, W. K. Tse, M. Kargarian, A. H. MacDonald, and G. Shvets, Photonic topological insulators, Nat. Mater. **12**, 233 (2013).
[2] C. Leefmans, A. Dutt, J. Williams, L. Yuan, M. Parto, F. Nori, S. Fan, and A. Marandi, Topological dissipation in a time-multiplexed photonic resonator network, Nat. Phys. **18**, 442 (2022).
[3] T. Ozawa, H. M. Price, A. Amo, N. Goldman, M. Hafezi, L. Lu, M. C. Rechtsman, D. Schuster, J. Simon, O. Zilberberg, and I. Carusotto, Topological photonics, Rev. Mod. Phys. **91**, 015006 (2019).
[4] X. Zhang, F. Zangeneh-Nejad, Z.-G. Chen, M.-H. Lu, and J. Christensen, A second wave of topological phenomena in photonics and acoustics, Nature (London) **618**, 687 (2023).
[5] C. He, X. Ni, H. Ge, X. C. Sun, Y. B. Chen, M. H. Lu, X. P. Liu, and Y. F. Chen, Acoustic topological insulator and robust one-way sound transport, Nat. Phys. **12**, 1124 (2016).
[6] H. Hu, S. Han, Y. Yang, D. Liu, H. Xue, G. G. Liu, Z. Cheng, Q. J. Wang, S. Zhang, B. Zhang, and Y. Luo, Observation of topological edge states in thermal diffusion, Adv. Mater. **34**, 2202257 (2022).
[7] Z. Liu, P. Jin, M. Lei, C. Wang, F. Marchesoni, J.-H. Jiang, and J. Huang, Topological thermal transport, Nat. Rev. Phys. **6**, 554 (2024).
[8] F. Yang, Z. Zhang, L. Xu, Z. Liu, P. Jin, P. Zhuang, M. Lei, J. Liu, J.-H. Jiang, X. Ouyang, F. Marchesoni, and J. Huang, Controlling mass and energy diffusion with metamaterials, Rev. Mod. Phys. **96**, 015002 (2024).
[9] R. Süsstrunk and S. D. Huber, Observation of phononic helical edge states in a mechanical topological insulator, Science **349**, 47 (2015).
[10] T. X. Dai, A. Q. Ma, J. Mao, Y. T. Ao, X. Y. Jia, Y. Zheng, C. H. Zhai, Y. Yang, Z. H. Li, B. Tang, J. Luo, B. L. Zhang, X. Y. Hu, Q. H. Gong, and J. W. Wang, A programmable topological photonic chip, Nat. Mater. **23**, 928 (2024).
[11] R. Keil, C. Poli, M. Heinrich, J. Arkinstall, G. Weihs, H. Schomerus, and A. Szameit, Universal sign control of coupling in tight-binding lattices, Phys. Rev. Lett. **116**, 213901 (2016).

[12] M. Golshani, S. Weimann, K. Jafari, M. K. Nezhad, A. Langari, A. R. Bahrampour, T. Eichelkraut, S. M. Mahdavi, and A. Szameit, Impact of loss on the wave dynamics in photonic waveguide lattices, Phys. Rev. Lett. **113**, 123903 (2014).
[13] S. Ryu and Y. Hatsugai, Topological origin of zero-energy edge states in particle-hole symmetric systems, Phys. Rev. Lett. **89**, 077002 (2002).
[14] P. Delplace, D. Ullmo, and G. Montambaux, Zak phase and the existence of edge states in graphene, Phys. Rev. B **84**, 195452 (2011).
[15] T. Yoshida and Y. Hatsugai, Bulk-edge correspondence of classical diffusion phenomena, Sci. Rep. **11**, 888 (2021).
[16] S.-D. Liang and G.-Y. Huang, Topological invariance and global Berry phase in non-Hermitian systems, Phys. Rev. A **87**, 012118 (2013).
[17] S. Weidemann, M. Kremer, S. Longhi, and A. Szameit, Topological triple phase transition in non-Hermitian Floquet quasicrystals, Nature (London) **601**, 354 (2022).
[18] G. G. Pyrialakos, J. Beck, M. Heinrich, L. J. Maczewsky, N. V. Kantartzis, M. Khajavikhan, A. Szameit, and D. N. Christodoulides, Bimorphic Floquet topological insulators, Nat. Mater. **21**, 634 (2022).
[19] S. Yin, E. Galiffi, and A. Alù, Floquet metamaterials, eLight **2**, 8 (2022).
[20] Y. Lumer, M. A. Bandres, M. Heinrich, L. J. Maczewsky, H. Herzig-Sheinfux, A. Szameit, and M. Segev, Light guiding by artificial gauge fields, Nat. Photonics **13**, 339 (2019).
[21] M. C. Rechtsman, J. M. Zeuner, Y. Plotnik, Y. Lumer, D. Podolsky, F. Dreisow, S. Nolte, M. Segev, and A. Szameit, Photonic Floquet topological insulators, Nature (London) **496**, 196 (2013).
[22] R. Fleury, A. B. Khanikaev, and A. Alù, Floquet topological insulators for sound, Nat. Commun. **7**, 11744 (2016).
[23] M. Jürgensen, S. Mukherjee, and M. C. Rechtsman, Quantized nonlinear Thouless pumping, Nature (London) **596**, 63 (2021).
[24] M. Lohse, Exploring 4D quantum Hall physics with a 2D topological charge pump, Nature (London) **553**, 55 (2018).
[25] O. Zilberberg, S. Huang, J. Guglielmon, M. Wang, K. P. Chen, Y. E. Kraus, and M. C. Rechtsman, Photonic topological boundary pumping as a probe of 4D quantum Hall physics, Nature (London) **553**, 59 (2018).
[26] R. Citro and M. Aidelsburger, Thouless pumping and topology, Nat. Rev. Phys. **5**, 87 (2023).
[27] Y. K. Sun, X. L. Zhang, F. Yu, Z. N. Tian, Q. D. Chen, and H. B. Sun, Non-Abelian Thouless pumping in photonic waveguides, Nat. Phys. **18**, 1080 (2022).
[28] M. Kim, Z. Jacob, and J. Rho, Recent advances in 2D, 3D and higher-order topological photonics, Light Sci. Appl. **9**, 130 (2020).
[29] B. Y. Xie, H. X. Wang, X. J. Zhang, P. Zhan, J. H. Jiang, M. H. Lu, and Y. F. Chen, Higher-order band topology, Nat. Rev. Phys. **3**, 520 (2021).
[30] M. Kim, Z. H. Wang, Y. H. Yang, H. T. Teo, J. Rho, and B. L. Zhang, Three-dimensional photonic topological insulator without spin-orbit coupling, Nat. Commun. **13**, 3499 (2022).
[31] H. Gao, H. R. Xue, Z. M. Gu, T. Liu, J. Zhu, and B. L. Zhang, Non-Hermitian route to higher-order topology in an acoustic crystal, Nat. Commun. **12**, 1888 (2021).
[32] M. Y. Li, D. Zhirihin, M. Gorlach, X. Ni, D. Filonov, A. Slobozhanyuk, A. Alù, and A. B. Khanikaev, Higher-order topological states in photonic kagome crystals with long-range interactions, Nat. Photonics **14**, 89 (2020).
[33] W. Wang, X. L. Wang, and G. C. Ma, Non-Hermitian morphing of topological modes, Nature (London) **608**, 50 (2022).
[34] Y. Li, C. Fan, X. Hu, Y. Ao, C. Lu, C. T. Chan, D. M. Kennes, and Q. Gong, Effective Hamiltonian for photonic topological insulator with non-Hermitian domain walls, Phys. Rev. Lett. **129**, 053903 (2022).
[35] J. D. H. Rivero, C. Fleming, B. Qi, L. Feng, and L. Ge, Robust zero modes in non-Hermitian systems without global symmetries, Phys. Rev. Lett. **131**, 223801 (2023).
[36] W. Song, W. Sun, C. Chen, Q. Song, S. Xiao, S. Zhu, and T. Li, Breakup and recovery of topological zero modes in finite non-Hermitian optical lattices, Phys. Rev. Lett. **123**, 165701 (2019).
[37] H. Wetter, M. Fleischhauer, S. Linden, and J. Schmitt, Observation of a topological edge state stabilized by dissipation, Phys. Rev. Lett. **131**, 083801 (2023).
[38] Z. Y. Feng and X. K. Sun, Harnessing dynamical encircling of an exceptional point in anti-PT-symmetric integrated photonic systems, Phys. Rev. Lett. **129**, 273601 (2022).
[39] M. Pan, H. Zhao, P. Miao, S. Longhi, and L. Feng, Photonic zero mode in a non-Hermitian photonic lattice, Nat. Commun. **9**, 1308 (2018).
[40] S. Lieu, Topological phases in the non-Hermitian Su-Schrieffer-Heeger model, Phys. Rev. B **97**, 045106 (2018).
[41] C. Poli, M. Bellec, U. Kuhl, F. Mortessagne, and H. Schomerus, Selective enhancement of topologically induced interface states in a dielectric resonator chain, Nat. Commun. **6** (2015).
[42] Q. Guo, T. Jiang, R.-Y. Zhang, L. Zhang, Z.-Q. Zhang, B. Yang, S. Zhang, and C. T. Chan, Experimental observation of non-Abelian topological charges and edge states, Nature (London) **594**, 195 (2021).
[43] Y. Yang, B. Yang, G. Ma, J. Li, S. Zhang, and C. T. Chan, Non-Abelian physics in light and sound, Science **383**, eadf9621 (2024).
[44] Y. Yang, C. Peng, D. Zhu, H. Buljan, J. D. Joanmopoulos, B. Zhen, and M. Soljacic, Synthesis and observation of non-Abelian gauge fields in real space, Science **365**, 1021 (2019).
[45] B. Jiang, A. Bouhon, Z. K. Lin, X. X. Zhou, B. Hou, F. Li, R. J. Slager, and J. H. Jiang, Experimental observation of non-Abelian topological acoustic semimetals and their phase transitions, Nat. Phys. **17**, 1239 (2021).
[46] H. H. Qiu, Q. C. Zhang, T. Z. Liu, X. Y. Fan, F. Zhang, and C. Y. Qiu, Minimal non-Abelian nodal braiding in ideal metamaterials, Nat. Commun. **14**, 1261 (2023).
[47] K. Wang, A. Dutt, C. C. Wojcik, and S. H. Fan, Topological complex-energy braiding of non-Hermitian bands, Nature (London) **598**, 59 (2021).
[48] M. P. Hokmabadi, N. S. Nye, R. El-Ganainy, D. N. Christodoulides, and M. Khajavikhan, Supersymmetric laser arrays, Science **363**, 623 (2019).

[49] A. Schumer, Y. G. N. Liu, J. Leshin, L. Ding, Y. Alahmadi, A. U. Hassan, H. Nasari, S. Rotter, D. N. Christodoulides, P. LiKamWa, and M. Khajavikhan, Topological modes in a laser cavity through exceptional state transfer, Science **375**, 884 (2022).
[50] L. C. Yang, G. R. Li, X. M. Gao, and L. Lu, Topological-cavity surface-emitting laser, Nat. Photonics **16**, 279 (2022).
[51] C. A. Rosiek, G. Arregui, A. Vladimirova, M. Albrechtsen, B. V. Lahijani, R. E. Christiansen, and S. Stobbe, Observation of strong backscattering in valley-Hall photonic topological interface modes, Nat. Photonics **17**, 386 (2023).
[52] A. B. Khanikaev and A. Alù, Topological photonics: Robustness and beyond, Nat. Commun. **15** (2024).
[53] I. L. Garanovich, S. Longhi, A. A. Sukhorukov, and Y. S. Kivshar, Light propagation and localization in modulated photonic lattices and waveguides, Phys. Rep. **518**, 1 (2012).
[54] C. E. Bardyn, M. A. Baranov, C. V. Kraus, E. Rico, A. İmamoğlu, P. Zoller, and S. Diehl, Topology by dissipation, New J. Phys. **15**, 085001 (2013).
[55] S. Longhi, Anderson localization in dissipative lattices, Ann. Phys. (Berlin) **535**, 2200658 (2023).
[56] S. Diehl, E. Rico, M. A. Baranov, and P. Zoller, Topology by dissipation in atomic quantum wires, Nat. Phys. **7**, 971 (2011).
[57] S. Mukherjee, D. Mogilevtsev, G. Y. Slepyan, T. H. Doherty, R. R. Thomson, and N. Korolkova, Dissipatively coupled waveguide networks for coherent diffusive photonics, Nat. Commun. **8**, 1909 (2017).
[58] D. Hao, L. Wang, X. Lu, X. Cao, S. Jia, Y. Hu, and Y. Xiao, Topological atomic spin wave lattices by dissipative couplings, Phys. Rev. Lett. **130**, 153602 (2023).
[59] W. Nie, M. Antezza, Y. X. Liu, and F. Nori, Dissipative topological phase transition with strong system-environment coupling, Phys. Rev. Lett. **127**, 250402 (2021).
[60] D. Porras and S. Fernández-Lorenzo, Topological amplification in photonic lattices, Phys. Rev. Lett. **122**, 143901 (2019).
[61] C. Gneiting, A. Koottandavida, A. V. Rozhkov, and F. Nori, Unraveling the topology of dissipative quantum systems, Phys. Rev. Res. **4**, 023036 (2022).
[62] Q. Zhang, C. Yang, J. Sheng, and H. Wu, Dissipative coupling-induced phonon lasing, Proc. Natl. Acad. Sci. U.S.A. **119**, e2207543119 (2022).
[63] A. Metelmann and A. A. Clerk, Nonreciprocal photon transmission and amplification via reservoir engineering, Phys. Rev. X **5**, 021025 (2015).
[64] Z. Dong, X. Chen, A. Dutt, and L. Yuan, Topological dissipative photonics and topological insulator lasers in synthetic time-frequency dimensions, Laser Photonics Rev. **18**, 2300354 (2024).
[65] T. Y. Chen, C. N. Weng, and J. S. Chen, Cloak for curvilinearly anisotropic media in conduction, Appl. Phys. Lett. **93**, 114103 (2008).
[66] S. Narayana and Y. Sato, Heat flux manipulation with engineered thermal materials, Phys. Rev. Lett. **108**, 214303 (2012).
[67] R. Hu, S. L. Zhou, Y. Li, D. Y. Lei, X. B. Luo, and C. W. Qiu, Illusion thermotics, Adv. Mater. **30**, 1707237 (2018).
[68] J. Guo, G. Q. Xu, D. Tian, Z. G. Qu, and C. W. Qiu, A real-time self-adaptive thermal metasurface, Adv. Mater. **34**, 2201093 (2022).
[69] J. Li, C. Xu, Z. Xu, G. Xu, S. Yang, K. Liu, J. Chen, and T. Li, Localized and delocalized topological modes of heat, Proc. Natl. Acad. Sci. U.S.A. **121**, e2408843121 (2024).
[70] C. Cao, R. Ju, D. Wang, M. Qi, K. Liu, G. Peng, and H. Chen, Observation of parity-time symmetry in diffusive systems, Sci. Adv. **10**, eadn1746 (2024).
[71] H. Wu, H. Hu, X. Wang, Z. Xu, B. Zhang, Q. J. Wang, Y. Zheng, J. Zhang, T. J. Cui, and Y. Luo, Higher-order topological states in thermal diffusion, Adv. Mater. **35**, 2210825 (2023).
[72] See Supplemental Material at http://link.aps.org/supplemental/10.1103/bk7q-6r9d which includes Refs. [2,11,16,55–57,63,73,74], for additional information about the detailed derivations of universal coupling control, the analysis of sensitive dynamics, and experimental methods.
[73] D. Mogilevtsev, G. Y. Slepyan, E. Garusov, S. Y. Kilin, and N. Korolkova, Quantum tight-binding chains with dissipative coupling, New J. Phys. **17**, 043065 (2015).
[74] C. Yin, H. Jiang, L. Li, R. Lü, and S. Chen, Geometrical meaning of winding number and its characterization of topological phases in one-dimensional chiral non-Hermitian systems, Phys. Rev. A **97**, 052115 (2018).
[75] C. C. Wanjura, M. Brunelli, and A. Nunnenkamp, Topological framework for directional amplification in driven-dissipative cavity arrays, Nat. Commun. **11**, 3149 (2020).
[76] L. Campos Venuti, Z. Ma, H. Saleur, and S. Haas, Topological protection of coherence in a dissipative environment, Phys. Rev. A **96**, 053858 (2017).
[77] P. St-Jean, V. Goblot, E. Galopin, A. Lemaître, T. Ozawa, L. Le Gratiet, I. Sagnes, J. Bloch, and A. Amo, Lasing in topological edge states of a one-dimensional lattice, Nat. Photonics **11**, 651 (2017).